AC conductance of quantum wires with inelastic scattering. I

AC conductance of quantum wires with inelastic scattering: I

V Špička, J Mašek and B Velický

Institute of Physics, Czechoslovak Academy of Science, Na Slovance 2, CS-18040 Praha 8, Czechoslovakia

Abstract. The influence of inelastic processes on the coherence in the semiballistic regime of mesoscopic transport is investigated by calculating the AC conductance of electrons in a single-channel quantum wire, coupled to a bath of longitudinal acoustic phonons. Numerical results illustrate the situation in GaAs structures.

1. Introduction

One of the outstanding experimentally established results in the area of mesoscopic transport is the quantisation of the DC conductance in very narrow constrictions fabricated in GaAs structures [1]. As the width of the constriction is varied, the conductance jumps by the universal value $2e^2/h$. This is interpreted in terms of quasi-one-dimensional electronic bands in the constriction, which define the conduction channels. Each band with a free Fermi surface yields an open channel whose contribution to the conductance is just $2e^2/h$, if the transport is purely ballistic. The spatial distribution of the applied electric field plays no role, only the total voltage.

These results were derived theoretically in various ways [2]. The theory was also extended to finite frequencies [3, 4]. Because of the fully quantal nature of this transport mode, the only adequate description is then the linear response theory, as represented by the Kubo formula. In [3, 4], it was applied to an ideal quantum wire (QW). This is a structure infinitely extended in one direction, but having a uniform finite cross section. Electrons in the wire are independent and ballistic: there is no scattering at all, elastic or inelastic. The constriction is simulated by a finite interval, to which a longitudinal electric field is applied; it causes a coherent motion of the electrons in the whole wire.

The linear response theory yields as a direct result the conductivity. In a homogeneous quasi-1D wire, the useful quantity is $\sigma(x - x', \omega)$ relating the local current $j(x)$ at position x with the field $\mathscr{E}$ of frequency ω acting at position x'. From this, we can calculate the empirically accessible conductance G defined by the power absorbed in the whole sample:

$$G \equiv G_\omega[\mathscr{E}] = \iint dx\, dx'\, \mathrm{Re}\, \sigma(x - x', \omega)\mathscr{E}(x)\mathscr{E}(x')\left(\int dx\, \mathscr{E}(x)\right)^{-2}. \quad (1)$$

The conductance incorporates only the absorptive part of the conductivity and it is a
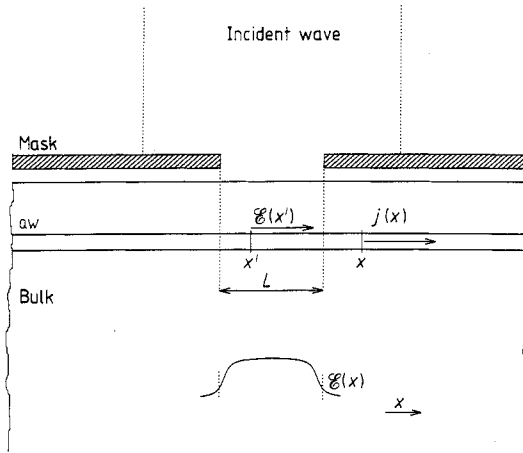
Figure 1. Quantum wire in an AC electric field. A microwave field incident on an opening in a shielding mask penetrates into the region of the QW just below as a longitudinal electric field acting on a finite interval L. A current density $j(x) = \int \mathrm{Re}\,\sigma(x - x')\mathscr{E}(x')\,\mathrm{d}x'$ is induced in the whole wire, but energy is absorbed only where the product $j(x)\mathscr{E}(x)$ is non-zero, that is in the intersection of the QW and the irradiated area between the dotted lines. The actual field distribution is not rectangular because of the diffraction on the diaphragm, as illustrated by the smooth plot at the bottom.

functional of the spatial distribution of the field amplitude $\mathscr{E}(x)$. Figure 1 sketches a possible scheme of an experiment in which a quasi-static longitudinal electric field in the microwave frequency range can be applied to a finite portion of the QW. Outside the wire, the sample is an insulator: all energy dissipation comes from the intersection of the irradiated region of the system with the QW.

An important result obtained in the coherent case is that at a finite frequency and for a homogeneous field $\mathscr{E}e^{-\mathrm{i}\omega t}$ acting on an interval of a length L, the one-channel conductance oscillates as

$$\sin^2(\omega L/2v_F)/(\omega L/2v_F)^2.$$

The DC limit does not depend on the field space variation.

Presently, we shall address the question: How sensitive is this behaviour to inelastic processes that tend to violate the ideal phase coherence of the electronic waves? This will be analysed first on a simple parametrised model for the conductivity (§ 2). As a next step towards a microscopic theory, we consider the inelastic scattering of electrons on longitudinal acoustic (LA) phonons (§ 3), obtain an approximation for the conductivity (§ 4), and the temperature dependence of the conductance in this case (§ 5).

2. Relaxation-time model for the conduction in non-ideal quantum wires

As a first step, we shall analyse (1) for a semiphenomenological model of conduction in one channel at zero electron temperature. With the assumption of a single relaxation time, the Kubo formula for the conductivity σ becomes

$$\sigma(x - x', \omega) = 2\frac{e^2}{h}\,e^{\mathrm{i}\alpha|x-x'|} \qquad \alpha = \frac{\omega + \mathrm{i}\tau^{-1}}{v_F} = \Lambda_\omega^{-1} + \mathrm{i}l_\varphi^{-1}. \qquad (2)$$

The relaxation time τ and the Fermi velocity v_F are parameters, and their combination
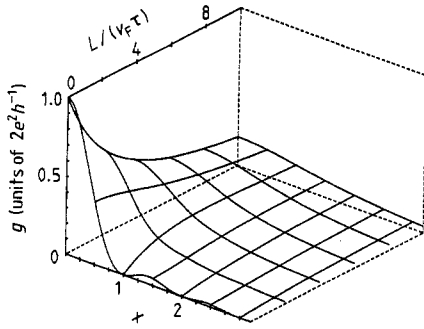
Figure 2. Single-channel conductance g in units of $2e^2h^{-1}$ according to equation (2). The dimensionless frequency $x = (\omega/2\pi)(L/v_F)$; dimensionless damping is $L/(v_F\tau)$.

τv_F defines the coherence length l_φ. Equation (2) contains, in addition to l_φ, another characteristic length $2\pi\Lambda_\omega = 2\pi v_F/\omega$, the wavelength of an electron–hole pair with the excitation energy $\hbar\omega$. The resulting conduction regime will depend on the interplay of these two lengths with one another and with the characteristic size of the spatial inhomogeneity of the electric field. As the simplest example, we choose the 'mesa' field, constant over a length L, considered already in [3, 4]. The normalised conductance g resulting from equations (1) and (2) in this case is

$$g = \frac{Gh}{2e^2} = \mathrm{Re}\left[-\frac{2}{i\zeta}\left(1 + \frac{1 - e^{i\zeta}}{i\zeta}\right)\right] \tag{3a}$$

$$\zeta = L\alpha = L/\Lambda_\omega + i\,L/l_\varphi \equiv \xi + i\eta \tag{3b}$$

and it depends on two dimensionless variables ξ, η given by the ratios of the characteristic lengths, which are called 'frequency' and 'damping' in figure 2.

The DC conductance is obtained in the limit $\Lambda_\omega \to \infty$. It appears in figure 2 as the leftmost curve running to the depth of the plot. In the coherent regime (zero damping, $l_\varphi \to \infty$), the conductance $g \to 1$ does not depend on L. This is the proper mesoscopic behaviour. For increasing damping, the Boltzmann equation limit is achieved, with the asymptotic form $g \sim 2v_F\tau/L$, in which g is inversely proportional to L. Thus, it obeys Ohm's law: the resistances of distant parts of the wire compose additively.

The frequency dependence of the conductance for various dampings has an analogous interpretation. The coherent limit is shown as the front profile in figure 2. The analytic form of the coherent $g(\omega)$ is the

$$\sin^2(\omega L/v_F)/(\omega L/v_F)^2$$

result [3, 4] mentioned already in § 1. It starts from the DC value of 1 and its most prominent features are the predicted zeros at integer ξ, that is when L is a half-integer multiple of Λ_ω. The characteristic frequency

$$\omega_0 = 2\pi v_F/L \tag{4}$$

corresponding, for a given L, to the first node at $\xi = 1$, will be called the node frequency.

As the damping is increased, $g(\omega)$ undergoes a gradual transition from oscillatory shape to the asymptote of a monotonic bell-shaped curve tending to the Drude formula behaviour.

Similar considerations are possible also for more complicated fields. We just mention that the basic conclusions for the mesa field are not altered if its edges are rounded [4].

Another case may be a field periodically modulated in space, resulting in the resonance-like form of $g(\omega)$. We want to pay more attention to the field acting along two intervals L separated by a zero-field region of length d. This special field configuration should lead to a new interference effect: with the natural assumption that the electrical field in both intervals is coherent, the conductances of both intervals will interfere in a fashion analogous to double-slit diffraction in optics, provided the electron waves have coherence length sufficiently large, $l_\varphi \gg d$. This interference effect will be largely suppressed as l_φ becomes comparable to d. This opens up a new possibility of direct observation of the degree of coherence, and of measuring l_φ. The double-mesa conductance is easily obtained as

$$g = \mathrm{Re}\,\tfrac{1}{2}\left[-\frac{2}{\mathrm{i}\zeta}\left(1 + \frac{1 - \mathrm{e}^{\mathrm{i}\zeta}}{\mathrm{i}\zeta}\right) + \left(\frac{1 - \mathrm{e}^{\mathrm{i}\zeta}}{\mathrm{i}\zeta}\right)^2 \mathrm{e}^{\mathrm{i}\zeta d/L}\right] \tag{5}$$

with ζ given by (3b). The first term in the square brackets is a 'single-slit' conductance (3a); the other term describes the interference effect. It is damped by $\exp(-\eta d/L) = \exp(-d/l_\varphi)$, which gives a quantitative estimate for the interference quenching. The total conductance is normalised by a factor of $1/2$: for $d \gg l_\varphi$, the resistance is an incoherent sum of the resistances of isolated intervals, each of which may still display an internal coherence. An illustration of these features will be given in § 4 using a quantitative estimate for τ based on a microscopic theory.

A concluding remark to this section may be that the approximation of a single relaxation time can be generalised to the case of several transport channels with individual v_F values. Their contributions to the conductance are simply summed.

3. Quantum wires modelling real structures in GaAs

To obtain actual estimates of τ, we shall consider a real situation in mesoscopic semiconductor structures [1].

3.1. Geometry of the QW and model electronic structure

As an example, we take the two-dimensional (2D) electron gas in a GaAs inversion layer. Additional gate electrodes with a narrow gap (constriction) create electrostatic barriers, which confine the electrons to a narrow, quasi-1D 'wire' with perfectly smooth 'walls'. Characteristic parameters of such a system [1, 5] are summarised in table 1.

It should be pointed out that the wire is embedded inside a 'bulk' sample, considered in the following as if it were 3D. The geometry of the wire is such that it permits one to work in the effective-mass approximation. In addition, we assume a parabolic conduction band, $\varepsilon(k) = \hbar^2 k^2/2m_c$. Then, for a homogeneous wire, we can write the electronic wavefunction in a separable form

$$\Psi_{k'}(r) \propto \mathrm{e}^{\mathrm{i}kx}\psi_\perp(r_\perp) \qquad r = (x, r_\perp) \tag{6a}$$

where $\psi_\perp$ defines the extent of the electron in the transverse direction. It depends on the confining potential. As the strength of the potential is increased, the wire becomes narrower and, consequently, the sub-bands move upwards, and the distances between the band edges increase. The number of open channels, i.e. the number of sub-bands crossed by the Fermi level E_F, is related to the electron concentration and to the

Table 1. Basic parameters of the model GaAs wire.

Material constants	
lattice spacing, a (nm)	0.5642
effective mass (cond. band), m_c/m_e	0.067
deformation potential, C (eV)	7.0
Geometrical characteristics	
extent of the electric field, L (μm)	10
transverse extent of the wavefunction, R (nm)	7
Characteristic energies	
Fermi level, E_F (meV)	20
energy equivalent to $T = 2$ K (meV)	0.17
node frequency, ω_0, for $L = 10\,\mu$m (GHz)	27
corresponding energy, $\hbar\omega_0$ (meV)	0.11
Other quantities	
Fermi velocity, v_F (m s^{-1})	2.7×10^5
velocity of sound, s (m s^{-1})	5.22×10^3

confinement. We take a fixed Fermi level, as is the case in the experiment. Under this condition, the cross section of the wire is the variable quantity controlling its transport properties. We are now interested in the single-channel case, when the Fermi level lies between the first and second lowest sub-band edges. It is clear that single-channel transport takes place in wires whose transverse dimensions are comparable (in contrast to the multichannel case realised in a 'flat' conductor). We assume a cylindrical wire, and of the two commonly used confining potentials, box-shaped and parabolic, we select the latter one. Then the ground-state transverse wavefunction is

$$\psi_\perp \propto e^{-0.5(r_\perp/R)^2} \tag{6b}$$

with the characteristic extent $R \le (\hbar^2/m_c E_F)^{1/2}$. For the presently considered situation, R is estimated to be 7 nm.

3.2. Interaction with LA phonons

At very low temperatures, the electrons scatter on static imperfections and on acoustic phonons, and also by mutual collisions. Scattering on imperfections is excluded by the conditions of preparation. Electron–electron scattering is neglected in the present approach. The only remaining interaction of importance is the coupling to the LA phonons by the deformation-potential mechanism.

   The electrostatic potential confining the electrons to the wire does not influence the lattice vibrations, and the phonons are not confined to the wire. This 3D nature of the phonon bath enables us to assume that it remains in its equilibrium state, which is not affected by the phonons emitted, absorbed by the electrons in the small volume of the wire. This makes the situation in the semiconductor structures different from the case of true metallic wires. The actual coupling between the 1D electrons and the 3D phonons is easily obtained by taking the matrix elements of the deformation potential, defined in the whole 3D space, in the basis Ψ_k of the electron eigenstates, which are, in the single-channel case, given by equations (6) and labelled by 1D wavevectors k.
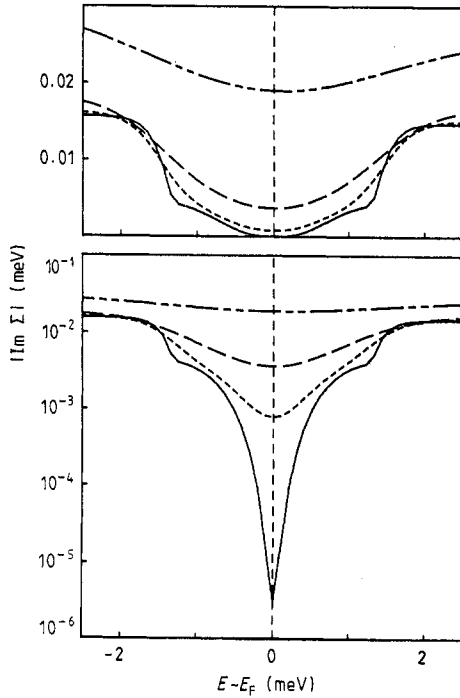
Figure 3. Imaginary part of the self-energy of electrons in GaAs moving in the ground channel and coupled by the deformation potential to LA phonons. Top panel: Im Σ for $k = 0.2$ nm^{-1} as a function of energy around the Fermi level $E_F = 20$ meV. Temperatures: (——) 0.3 K, (-----) 2 K, (— — —) 4 K, (—·—·—) 10 K. Bottom panel: the same in semi-logarithmic scale.

The effect of the electron–phonon interaction on the equilibrium electronic structure is described by the electron self-energy $\Sigma(k, E)$. For the electrons in the ground subband the self-energy is a scalar quantity depending on the 1D wavevector k. It is evaluated in the usual Migdal approximation [6],

$$\Sigma = i\hbar C^2 \mathcal{G} \mathcal{D} \tag{7}$$

where $\mathcal{G}$ and $\mathcal{D}$ are the Green functions of the electrons and the phonons, respectively. C is the deformation-potential coupling constant ($C = 7$ eV, table 1). The details of the evaluation of Σ are postponed to a future publication [7]. The main results are as follows. For temperatures up to 10 K, all renormalisation effects are negligible. The k dependence of Σ is rather weak, at least for the important k-vectors around k_F, as expected [6]. This substantially simplifies the formulation of the transport theory in the next section. The electron damping Im $\Sigma(k, E - i0)$ for $k = 0.2$ nm^{-1} is shown in figure 3 as a function of the energy for several temperatures $T \leqslant 10$ K. There, Im Σ never exceeds 0.03 meV. For low temperatures, this rather small quantity is further strongly reduced around the Fermi energy. This pronounced dip resembles the well known situation in metals [8] and confirms the validity of a 1D Luttinger theorem at $T \rightarrow 0$.

4. Linear response

In this section we first derive the Kubo formula appropriate for the present problem and show how the formal structure of the expression for $\sigma(x, \omega)$ used in § 2 comes out. The microscopic transport theory yields the relation between the transport relaxation time τ, used in § 2, and the imaginary part of the self-energy, obtained in § 3. The reasoning

in the 1D case is rather analogous to the analysis made by Holstein [9] in his classical work on metals.

We are studying the linear current response to a monochromatic electric field. The quantity needed in equation (1) for calculating the conductance is the absorptive part of the non-local conductivity $\sigma(x, \omega)$, which can be obtained as a Fourier transform

$$\sigma(x - x', \omega) = \int \frac{d\kappa}{2\pi} \sigma(\kappa, \omega)\, e^{i\kappa(x - x')} \tag{8}$$

of the susceptibility $\sigma(\kappa, \omega)$ measuring the linear response to a single Fourier component $\mathcal{E}_\kappa$ of the applied field,

$$\mathcal{E}(x, t) = \int \frac{d\kappa}{2\pi} \mathcal{E}_\kappa\, e^{i(\kappa x - \omega t)}. \tag{9}$$

We use the vector gauge with the vector potential

$$\mathcal{A}(x, t) = \frac{i}{\omega + i0}\, \mathcal{E}(x, t). \tag{10}$$

The diamagnetic term is purely imaginary and does not contribute to the absorptive (real) part of the conductivity. A major simplification we introduce in the present work (but not in the forthcoming paper [7]) is to neglect the transport vertex in the Kubo formula for the 1D conductivity, which becomes

$$\sigma(\kappa, \omega) = he^2 \int \frac{dE}{2\pi} \int \frac{dk}{2\pi} \left(\frac{f_- - f_+}{\hbar\omega} \right) v_k \mathcal{U}_+ v_k \mathcal{U}_- \tag{11a}$$

$$f_{\pm} = f(E \pm \hbar\omega/2) \qquad \mathcal{U}_\pm = \mathcal{U}(k \pm \kappa/2, E \pm \hbar\omega/2). \tag{11b}$$

Here $v_k = \hbar k/m_{\mathrm{eff}}$ is the electron velocity corresponding to the wavevector k, $f(u) = \{1 + \exp[\beta(u - E_{\mathrm{F}})]\}^{-1}$, and $\mathcal{U}(k, E)$ is the one-electron spectral function. It should be pointed out that the incorporation of the vertex correction would lead to a replacement of one of the v_k by a properly renormalised quantity.

The spectral function $\mathcal{U}(k, E)$ is the imaginary part of the equilibrium Green function,

$$\mathcal{U}(k, E) = \mp \pi^{-1} \mathrm{Im}[E \pm i0 - \varepsilon(k) - \Sigma(k, E \pm i0)]^{-1}. \tag{12}$$

It was noted already in § 3.2 that the k dependence of the self-energy $\Sigma(k, E)$ is rather weak. We neglect it completely in order to simplify the integration over k and to obtain a compact expression for the conductivity. We also neglect the real part of $\Sigma(k, E)$, which is a smooth function of the energy close to the Fermi level, and only weakly modifies the bare dispersion law $\varepsilon(k)$. This means that we define a real quantity $\Gamma(E)$ replacing the self-energy in (12):

$$\Sigma(k, E \pm i0) \to \mp i\Gamma(E) \qquad \Gamma(E) \geq 0. \tag{13}$$

The corresponding approximate form of the spectral function is

$$\mathcal{U}(k, E) = \frac{\Gamma(E)/\pi}{[E - \varepsilon(k)]^2 + [\Gamma(E)]^2}. \tag{14}$$

This approximation turns the integrand in the Kubo formula into a rational function of k. The integration over k can then be carried out explicitly. This is particularly easy if

the Fermi energy is large compared to all other characteristic energies: kT, $\hbar\omega$, $\hbar\omega_0$. This condition is valid in our case; it would fail for E_F close to the sub-band edge, when all this approach would be doubtful from the beginning. Holstein [9] also reduced the Kubo formula along similar lines. The present 1D case makes all steps much more transparent and simple. The very important feature common to Holstein's and our procedures is that there are no conditions on the relative magnitude of the 'small' characteristic energies, including a parameter measuring the energy variation of the self-energy. In other words, no approximation of the quasi-particle type, requiring poles in $\mathcal{G}$, appears here.

The integration in (11*a*) and (8) leads to the final result

$$\sigma(x - x', \omega; \beta, E_F) = 2\frac{e^2}{h} \int dE\, W_F(E, \omega)\, e^{i\alpha(E,\omega)|x - x'|} \tag{15}$$

with

$$\alpha(E, \omega) = [\omega + i\tau^{-1}(E, \omega)]/v(E) \qquad v(E) = (2E/m_c)^{1/2} \tag{16}$$

and

$$\tau^{-1}(E, \omega) = \hbar^{-1}[\Gamma_+ + \Gamma_-) \qquad \Gamma_\pm = \Gamma(E \pm \hbar\omega/2). \tag{17}$$

Finally, using the notation of equation (11*b*),

$$W_F(E, \omega) = (f_- - f_+)/\hbar\omega. \tag{18}$$

The familiar thermal weight function $W_F(E, \omega)$ is positive everywhere, but practically zero outside an interval around E_F of width $kT + \hbar\omega \ll E_F$. In the DC limit $\hbar\omega \to 0$, W_F reduces to $-df(E)/dE$; for all ω, its integral $\int dE\, W_F = 1$. The Kubo formula (15) yields the total conductivity as an inhomogeneous mixture of partial conductivities having the form of the phenomenological conductivity (2). If $\alpha(E, \omega)$ did not depend on the energy we would have a single relaxation time and (15) would reduce to (2). The energy dependence enters the microscopic expression (16) for $\alpha(E, \omega)$ through $v(E)$ and through the Γ quantities. The velocity $v(E)$ depends, in fact, little on E, so that the energy dependence of the damping $\Gamma(E)$ alone is responsible for the inhomogeneous broadening effect in the conductivity. The averaged quantity is the partial conductivity, not τ. Therefore, a thermally averaged relaxation time $\langle\tau\rangle$ or a coherence length $\langle l_\varphi\rangle$ can be, strictly speaking, introduced only in an effective sense, depending on the selected observable quantity, e.g. the DC conductance.

At $\omega \neq 0$, the relaxation time $\tau(E, \omega)$ is given by a 'Wigner' combination of the dampings corresponding to the initial and final states connected by a quantum $\hbar\omega$. To see the nature of our τ, consider the static case: $\tau(E, 0) = \hbar/2\Gamma(E)$. This would correspond, in a quasi-particle approximation ($\Gamma(E)$ practically independent of E), to the particle lifetime, and to the transport relaxation time in a 1D Boltzmann equation with the carrier back-scattering term omitted. This is consistent with the neglect of the transport vertex in the Kubo formula.

We do not use any form of a quasi-particle approximation. If we did this, the Kubo formula (11) would not go beyond the phenomenological model, as mentioned above, and it would be equivalent to the quasi-classical Boltzmann–Drude-like theory. In the present case, we see from figure 3 that $\Gamma(E)$ depends strongly on energy around E_F so that it is essential to use the generalised theory and to work with the full Kubo formula. Scattering on low-temperature phonons differs, in this respect, from elastic scattering
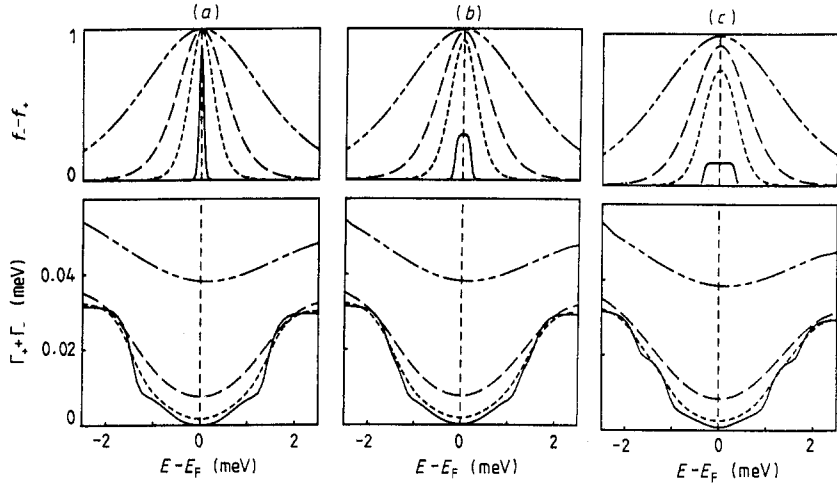
Figure 4. Inverse relaxation time (equation (17), bottom panel) and the weighting function (equation (18)) defining the temperature dependence of the conductance (top panel). The weighting functions are normalised as described in the text. The temperatures are indicated in the same way as in figure 3. (a) $\hbar\omega = 0.03$ meV, (b) $\hbar\omega = 0.33$ meV, (c) $\hbar\omega = 0.66$ meV.

on impurities, and also from quasi-elastic scattering by the phonons at higher temperatures. In both the latter cases, E_F is not accompanied by a singularity of Σ.

These general conclusions are illustrated for our GaAs wire in figure 4. For each temperature, the imaginary part of $\alpha(E, \omega)$ is calculated from the self-energies of figure 3. Above these plots, we draw the weighting function $W_F(E, \omega)$. It is normalised so that for all temperatures the values plotted are bounded by unity. The area below the curve for a given T is then $4k_BT$. The three frequencies considered are: the highest frequency in figure 2, $3\hbar\omega_0 \simeq 0.33$ meV (cf table 1); a frequency 10 times less, which may be thought to represent the DC limit, and finally, a 'high' frequency $6\hbar\omega_0$. In the DC case (figure 4(a)), the misalignment of the energy arguments is small, and the weight W_F is rather close to the derivative of the Fermi distribution already for the lowest temperature considered. The inverse relaxation time $\hbar\tau^{-1}$ nearly coincides with twice the single-particle self-energy. These two effects in conjunction mean that the low-temperature DC conductivity corresponds to coherent transport. As the temperature is increased, the effective coherence length rapidly decreases because, on the one hand, the self-energy is nowhere really small and, on the other hand, the side-wings of the increasingly broad weight function sample the regions far from E_F where $\Gamma = |\text{Im }\Sigma|$ is already not reduced by the Luttinger mechanism.

The higher frequencies and k_BT for the lowest temperatures are comparable, as is visualised by the shape of W_F, basically a rectangle with thermally rounded edges in figures 3(b) and (c). Also the structure of Im $\alpha(E, \omega)$ is now changed: the low-temperature self-energy varies sharply enough in E to cause the doubling of the kink structure of the self-energy, as well as an increase of Im $\alpha(E, \omega)$ around E_F, where it never gets very close to zero. At $3\hbar\omega_0$ ($\sim$0.33 meV), the change in $\alpha(E, \omega)$ is still not very conspicuous, but the high frequency $6\hbar\omega_0$ ($\sim$0.66 meV) is already comparable with the width of the self-energy dip around E_F, and Im $\alpha \simeq \Gamma_+ + \Gamma_-$ becomes flat around E_F. The degree of low temperature coherence thus decreases with increasing frequency.
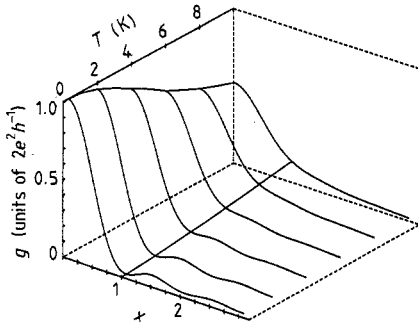
Figure 5. Single-channel conductance g in units of $2e^2h^{-1}$ as a function of dimensionless frequency $x = (\omega/2\pi)(L/v_F)$ for various temperatures T, as obtained from equation (15) for self-energies of figure 3. The homogeneous longitudinal field acts in an interval $L = 10\,\mu$m. Value $x = 1$ corresponds approximately to 27 GHz for GaAs and parameters given in table 1.

At this and still higher frequencies, like in the far-infrared region, no coherence effects are expected. For higher temperatures, the frequency effects are, of course, less pronounced.

5. Examples of conductance in GaAs QW

This final section is devoted to calculating the AC conductance for our microscopic model of a GaAs QW; most parameters have already been introduced, more or less as dictated by the system itself. They are summarised in table 1. The only remaining free quantity, the characteristic length L discussed in detail in § 2, is selected to be $10\,\mu$m. This fixes the node frequency $\omega_0 = 2\pi\nu_0$ to $\nu_0 = 27$ GHz, a value corresponding to the 0.11 meV referred to already in the preceding section.

In the following, we shall consider the two simple cases whose geometry and properties were discussed on a phenomenological level in § 2, namely the mesa field and the double-mesa field.

5.1. Conductance for the mesa field

The frequency and temperature dependences of the conductance are summarised in figure 5, which is arranged in the same way as figure 2. The frequency unit is fixed now to the specific value of ω_0 corresponding to 27 GHz, while the third axis measures the temperature rather than the dimensionless damping. Clearly, the effective damping increases with temperature and the transition from the mesoscopic oscillations to a monotonic Drude behaviour takes place similarly to figure 2. This similarity offers a procedure to define the effective coherent length $l_\varphi(T)$. For a fixed frequency, the conductance versus temperature dependence in figure 5 is mapped onto the conductance as a function of the damping in figure 2. The result of such transformation is shown in figure 6. The full curve relates to the DC conductance, the other one applies to the node frequency. In analysing these curves, it should first be observed that they are nearly identical except for small deviations at the lowest temperatures, indicating that this l_φ is an objective characteristic of the transport in a wide frequency range. This is in agreement with the discussion of frequency effects in figure 4. Secondly, we see that l_φ decreases steeply with increasing temperature, which corresponds to the transition from the coherent to the incoherent transport mode in figure 5. Quantitatively, this temperature dependence is given by a power law $l_\varphi \sim T^{-p}$. The full curve is fitted by $p =$
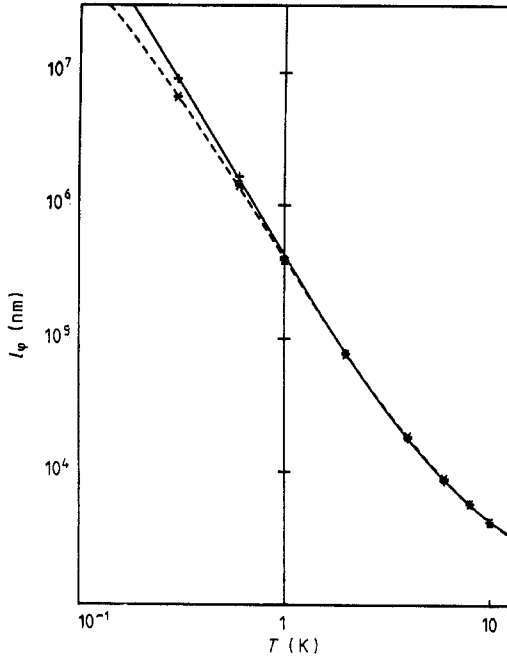
Figure 6. The temperature dependence of the coherence length l_φ obtained by fitting the results of figure 5 to equation (2). Full curve, DC case; broken curve, $\hbar\omega = 0.11$ meV (first node frequency).

$2.526 - 0.216T - 0.316T^2$. This should be compared with the exponent ranging from 3 to 4 in bulk metals [10].

Finally, the magnitude of l_φ appears to be of the order of micrometres or larger. These values are large, which could point to the importance of an additional scattering mechanism. However, we consider a single-channel case where the scattering efficiency of phonons is weakened by two factors: the very low number of final states, and the small overlap with the quasi-1D electron waves. The picture may easily change for, e.g., 10 channels open. It should be noted that the inclusion of the vertex correction in the Kubo formula, physically meaning accounting for the back-scattering of electrons, is expected to enhance rather than to reduce the coherence length.

5.2. Conductance for the double mesa field

The double mesa field, the other case considered on a phenomenological level in § 2, is illustrated in figure 7 by selected results obtained quantitatively on the basis of the microscopic theory. The conductance depends on several characteristic lengths in the system. The L value is fixed again as 10 μm. The variable length parameter in figure 7 is the gap size d. Two vertical sequences are obtained for two different temperatures; the temperature effect can be interpreted in terms of l_φ. According to figure 6, the temperatures of 2 and 4 K adjust l_φ to something like 80 and 20 μm, respectively. There is a fast decline in the coherence between 2 and 4 K. For 2 K, the interference oscillations predicted in § 2 are pronounced, while for the higher temperature they are more or less washed out. In the case $d \gg l_\varphi$ ($d \to \infty$, the bottom panels in figure 7), the total conductance is just one-half of the conductance in figure 5 corresponding to the single mesa case.
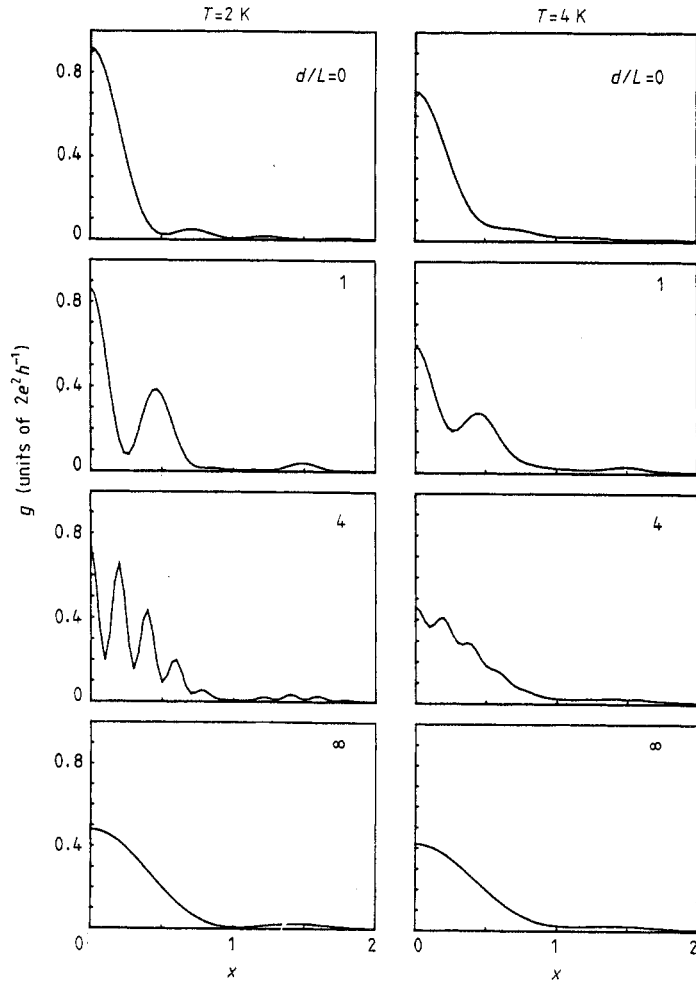
Figure 7. Single-channel conductance g in units of $2e^2h^{-1}$ as a function of dimensionless frequency $x = (\omega/2\pi)(L/v_F)$. The homogeneous longitudinal field acts in two intervals ($L = 10\,\mu m$) separated by a zero-field region of length d as indicated. Value $x = 1$ corresponds approximately to 27 GHz. Left part, $T = 2$ K; right part, $T = 4$ K.

Figure 7 can be read also in the horizontal direction closely corresponding to a realistic experimental arrangement with a fixed geometry of the field and a variable temperature, which could serve for a direct measurement of the coherence length.

6. Conclusions

We studied the frequency-dependent conductance of a model quasi-1D conductor with the aim of describing the transition from the quantum ballistic to an incoherent transport regime caused by the inelastic phase breaking processes. For a relaxation-time model, the conductance was expressed analytically as a function of three characteristic lengths, namely the coherence length, the spatial extent of the exciting field and the wavelength

of the excited electron–hole pair. The formulae are illuminating for the basic under-standing of the effect of partial coherence.

To describe these effects on a microscopic level, we considered a thin quantum wire in a GaAs structure in which the degenerate non-interacting carriers occupied only one sub-band and were coupled to the longitudinal acoustic phonons. With acceptable assumptions, the Kubo formula for the non-local conductivity was reduced to the form of thermally averaged elementary conductivities whose effective coherence lengths were related to the imaginary part of the electron self-energy. The coherent mode of the low-temperature conduction was thus explained by two simultaneous factors: a narrow area around the Fermi level for the thermal averaging, and the very small values of $|\text{Im }\Sigma|$ in this energy range caused by the selection rules for the phonon emission (Luttinger mechanism). At higher temperatures, both the incoherence thermal averaging and the increased phonon concentration tend quickly to suppress the coherence.

Relating the explicit results for the conductance to the phenomenological formulae, we were able to define the temperature-dependent coherence length. The dependence can be fitted by a power law. In a wide temperature range, the exponent is insensitive to the AC field frequency for which the fit is done.

It should be pointed out that the single-channel model is exceptional in yielding very low scattering rates because of a small number of available final states in the one-channel case and a small overlap between electrons and phonons. This leads to the large l_φ in figure 6. The next step in the theory should be the multichannel case. Other important problems not considered in the present work are the full self-consistency and the inclusion of the transport vertices, which can both modify the behaviour of the con-ductance. Also electron–electron scattering is necessary for the theory to become real-istic. An improved theory will be detailed in a subsequent paper [7].

References

[1] van Wees B J, van Houten H, Beenaacker C W J, Williamson J G, Kouwenhoven L P, van der Marel D, Foxon C T 1988 *Phys. Rev. Lett.* **60** 848
   Wharam D A, Thornton T J, Newbury R, Pepper M, Ahmed H, Frost J E F, Hasko D G, Peacock D C, Ritchie D A, Jones G A C 1988 *J. Phys. C: Solid State Phys.* **21** L209
[2] Isawa Y 1988 *J. Phys. Soc. Japan* **57** 3457
   Johnston R and Schweitzer L 1988 *J. Phys. C: Solid State Phys.* **21** L681
[3] Mašek J and Kramer B 1989 *Z. Phys.* B **75** 37
[4] Velický B, Mašek J and Kramer B 1989 *Phys. Lett.* to appear
[5] Fawcett W, Boardman A D and Swain S 1970 *J. Phys. Chem. Solids* **31** 1963
[6] Prange R E and Kadanoff L P 1964 *Phys. Rev.* **134** A566
[7] Velický B, Špička V and Mašek J in preparation
[8] Mahan G D 1981 *Many Particle Physics* (New York: Plenum)
[9] Holstein T 1964 *Ann. Phys., NY* **29** 410
[10] Schmid A 1985 in *Localisation, Interaction and Transport Phenomena* ed. B Kramer, G Bergmann and Y Bruynseraede, Springer Series in Solid-State Sciences, Vol 61 (New York: Springer) p 212